Fixed-mass multifractal analysis of river networks and braided channels

Samuele G. De Bartolo,[1,*] Leonardo Primavera,[2,†] Roberto Gaudio,[1,‡] Antonino D'Ippolito,[1,§] and Massimo Veltri[1,‖]
[1]*Dipartimento di Difesa del Suolo "V. Marone," Università della Calabria, P. Bucci 42b, Rende I-87030, Italy*
[2]*Dipartimento di Fisica, Università della Calabria, P. Bucci 33b, Rende I-87030, Italy*
(Received 11 January 2006; revised manuscript received 10 June 2006; published 2 August 2006)

A fixed-mass multifractal (FMA) analysis was used to investigate natural river networks and braided channels. In particular, while the study of natural river networks was performed with fixed-size algorithms (FSAs) in the past, the analysis of natural braided channels was not pursued before to our knowledge. Results showed the multifractal and non-plane-filling nature of all the digitalized data sets. Analysis of the digitalization step (constant or not) was performed and showed that it does not exert a strong influence on the assessed values of the Lipschitz-Hölder exponents and the support dimensions, even if a constant step permits better reconstruction of the right sides of the spectra, for negative moment orders of probabilities. The FMA approach presented two improvements with respect to the FSA one, in terms of oscillations of the scaling curves for negative moment orders of probabilities and of error bars. A more precise assessment of the multifractal spectra is of great importance in the development of multifractal models for the simulation of flood hydrographs.

DOI: 10.1103/PhysRevE.74.026101 PACS number(s): 89.75.Da, 03.50.−z, 92.40.Ea

I. INTRODUCTION

The multifractal analysis is a powerful tool in many fields of science. In the last 30 years, since the pioneering works by Mandelbrot [1], Grassberger [2], Grassberger and Procaccia [3], Hentschel and Procaccia [4], Schertzer and Lovejoy [5], Badii and Politi [7], and Frisch and Parisi [8], several contributions have been given to many branches of physics, chemistry, engineering, medicine, biology, ecology, geography, finance, etc. In particular, in hydrology the study of river basins and networks has produced innovative results, broadening the monofractal view of the scale properties of many relevant hydrological variables [9,10] and improving the assessment of the hydrologic response of a basin [11,12].

In the last ten years, much research was carried out, leading to some important conclusions: the projections of river networks on topographic maps are multifractal objects [10]; their support fractal dimension is less than 2 (non-plane-filling structures) [10,13,14]; their multifractal spectra can be obtained for both positive (left side of the spectra) and negative (right side of the spectra) moment orders of probabilities [15]; the hydrologic response of a basin (flood hydrograph) can be assessed with high precision, by using the multifractal instantaneous unit hydrograph [11,12].

The assessment of the multifractal spectrum is usually performed numerically, through generalized fixed-size algorithms (FSAs) or fixed-mass algorithms (FMAs). The first are appropriate for multifractals in which the original region is initially divided into several pieces; then, at each step, each piece is subdivided into other pieces, the size of which is reduced by a constant factor. On the other hand, the second type, introduced by Badii and Politi [7], are appropriate if the measure of each piece is reduced by a constant factor [16].

In some previous work of our research group, only FSAs were considered: in particular, the sandbox method and the generalized correlation integral method [19]. It was shown that both methods are able to (1) reconstruct the multifractal spectrum for both left and right sides; (2) avoid the border effects that emerge in the application of box-counting algorithms when the boxes present few points not centered in them; (3) discover the multifractality of natural river networks; and (4) recognize their non-plane-filling structure.

In the present work, applications of a FMA to natural river networks are presented. The analysis was pursued on both dendritic drainage patterns (basin scale) and braided channel patterns (channel scale). It is to be noted that the complexity of river networks and braided channels is different. In fact, river networks are assimilated to tree graphs and braided channels to cyclic graphs, and it is well known in the geomorphologic and hydrologic literature that they present different values of geomorphological descriptors (e.g., the *average junction degree* is about 2 for river networks and 3 for braided channels) (see, e.g., [20]). Therefore, the hypothesis of multifractality for braided channels needs verifying.

II. MULTIFRACTAL TECHNIQUES: FIXED-SIZE AND FIXED-MASS ALGORITHMS

A general multifractal analysis technique for an experimental set of data is based on the investigation of the scaling properties of the set of points. Let F be a fractal geometric object (the river network or the braided channels under study, in our case), defined upon an n-dimensional geometrical support. From the geometric map of this set we extract, in a regular manner that will be specified later, Q sequences of N_t points, representative of the fractal object. Hence, the evaluation of the fractal dimension of the set is performed through the following procedure. Each sequence of points is covered with N_c nonoverlapping cells, with side size ε_i, $1 \leqslant i \leqslant N_c$.

*Electronic address: debartolo@dds.unical.it
†Electronic address: lprimavera@fis.unical.it
‡Electronic address: gaudio@unical.it
§Electronic address: dippoli@dds.unical.it
‖Electronic address: veltrim@dds.unical.it

Let p_i be the measure (or probability or mass) in the ith box of the partition, namely, the ratio between the number of points of the set which fall into it, N_i, and the total number of points, N_t, of the sequence. This normalized quantity obviously depends on the size ε_i of the partition; however we drop this dependence in the formulas to avoid weighing down the notation. It is possible to show that the following relation holds [21]:

$$\lim_{\varepsilon_i \to 0} \left\langle \sum_{i=1}^{N_c} (p_i^{q-1} \varepsilon_i^{-\tau_q}) \Big/ N_c \right\rangle_Q = k \tag{1}$$

where k is a constant and q and τ_q are real numbers. The average operation $\langle \cdot \rangle_Q$ represents an ensemble average over each of the Q extracted sequences.

Equation (1) does not converge to a constant value for whatever q and τ_q, but only for particular values which are related to the "local" fractal dimension of the set. The multifractal analysis of the object is then performed by seeking for the values of q and τ_q that satisfy relation (1). We notice here that, when dealing with experimental data, it is not always possible to have several extractions of data points, but, in most cases, just a single one ($Q=1$). If this occurs, one can drop the ensemble average in (1). Finally, the goal of the investigation is accomplished by finding the values of q and τ_q which satisfy the following relation [21]:

$$\lim_{\varepsilon_i \to 0} \frac{\sum_{i=1}^{N_c} (p_i^{q-1} \varepsilon_i^{-\tau_q})}{N_c} = k. \tag{2}$$

Once the dependence of τ_q on q has been established, the generalized fractal dimensions D_q of the set can be obtained through the well-known formula [4]

$$D_q = \frac{\tau_q}{(q-1)} \quad \forall\, q \neq 1, \tag{3}$$

while the so-called Lipschitz-Hölder exponents α_q and the multifractal spectrum $f(\alpha_q)$ are given by the relations [22]

$$\alpha_q = \frac{d\tau_q}{dq}, \quad f(\alpha_q) = q\alpha_q - \tau_q. \tag{4}$$

Thus, when the determination of τ_q is accomplished, other meaningful quantities for establishing the multifractal properties of the set are obtained by interpolating the behavior of τ_q through suitable polynomials and then using Eqs. (3) and (4).

However, what characterizes different multifractal algorithms is the way through which the dependence of τ_q on q is sought.

In the so-called fixed-size algorithms, the determination of τ_q is carried out by fixing the size of the boxes covering the set, namely, $\varepsilon_i = \varepsilon \ \forall i$. In this case, the factor ε in (2) is independent of i and can be factorized, to get [21]

$$\lim_{\varepsilon \to 0} \left(\sum_{i=1}^{N_c} p_i^{q-1} \Big/ N_c \right) \varepsilon^{-\tau_q} = \lim_{\varepsilon \to 0} M(\varepsilon, q) \varepsilon^{-\tau_q} = k, \tag{5}$$

where $M(\varepsilon, q) = \Sigma_i p_i^{q-1} / N_c$ represents the moment of order $q-1$ of the measure.

Taking the term $\varepsilon^{-\tau_q}$ on the right-hand side of Eq. (5) and considering the logarithms of both terms, the previous equation becomes [21]

$$\lim_{\varepsilon \to 0} \ln M(\varepsilon, q) = \tau_q \lim_{\varepsilon \to 0} \ln \varepsilon + \ln k. \tag{6}$$

In practice the method consists, for each value of q, in fixing a set of decreasing values for the side ε of the boxes covering the data set. The measure in the ith box, $p_i(\varepsilon)$, depends on the side ε of the box. Once this quantity is computed, its $(q-1)$th order moment $M(\varepsilon, q)$ can be evaluated. The value of τ_q is then obtained by fitting the linear part of $\ln M(\varepsilon, q)$ vs $\ln \varepsilon$.

The complexity of the most optimized FSAs is $O(N_t \log_2 N_t)$ (see, e.g., [6]).

This kind of approach has a major drawback in the fact that, for negative values of q, the boxes populated by a low number of points give a high contribution to the moments and produce oscillations in the scaling for small values of ε. This problem is particularly evident when using the standard FSA box-counting method; nevertheless, some specific FSAs can overcome this difficulty, as shown in some applications to river networks of the sandbox method [17,19] and the generalized correlation integral method [18,19].

The so-called fixed-mass algorithms are an alternative to the FSAs, being very effective in reconstructing the right side of the multifractal spectrum for $q < 0$. In the FMAs, the quantity held fixed is no longer the size ε_i of the covering boxes, but rather the measure p_i inside the ith box, namely, $p_i = p \ \forall i$ (i.e., $N_i = N \ \forall i$). In this case, instead of searching for the dependence of τ_q on q, the behavior of q as a function of τ_q is sought. That is, when $p_i = p$ is held fixed, the term p^{q-1} can be factorized in (2) and taken to the second hand, by yielding the relation [7]

$$\lim_{\varepsilon_i \to 0} \frac{\sum_{i=1}^{N_c} \varepsilon_i^{-\tau_q}}{N_c} = k p^{1-q},$$

that is, by defining the quantity $M(\varepsilon_i, \tau_q) = \Sigma_i \varepsilon_i^{-\tau_q} / N_c$ and taking the logarithms of both members of the equation [21],

$$\lim_{\varepsilon_i \to 0} \ln M(\varepsilon_i, \tau_q) = (1-q) \lim_{p \to 0} \ln p + \ln k \tag{7}$$

where it has been taken into account that when ε_i tends to 0, p does also.

In the present work, the FMA algorithm was implemented in the following way. An interval of values for τ_q was chosen; for each τ_q we fixed a set of decreasing values of p. Given a p, for each point x_i of the data set the distances $d(x_i, x_j)$ between x_i and the generic point x_j were found and sorted in increasing order. The pth $d(x_i, x_j)$ of this list of values represented the diameter of a circle containing p points, namely, the value of ε_i for the point under consider-

ation. The moment $M(\varepsilon_i, \tau_q)$ was then computed and, from the scaling of $\ln M(\varepsilon_i, \tau_q)$ vs $\ln p$, the values of the angular coefficient in (7), $(1-q)$, were obtained, and, finally, the value of q corresponding to the given τ_q was found. By inverting the relation $q=q(\tau_q)$, we assessed the behavior of τ_q as a function of q, along with the other related quantities through Eqs. (3) and (4).

This numerical procedure has a complexity of $O(N_t^2 \log_2 N_t)$ and, therefore, can be more time consuming than using optimized FSAs. For this reason many authors, instead of considering the whole set of data points, took into account only the distances between an ensemble of randomly extracted data points from the original set and the remaining points (see, e.g., [7]). However, this procedure speeds up the computational time but it might influence the precision of the results. Therefore, we preferred not to use this modification of the algorithm, also considering that the CPU speed of current personal computers has increased with respect to the past.

III. FMA APPLICATIONS TO RIVER NETWORKS AND BRAIDED CHANNELS

We applied the FMA described above to some natural river networks and braided channels of the Calabria region (Italy). The study cases were the Ancinale, Corace, Crati, Petrace, and Trionto river networks and the braided channels of an about 10 km-long reach of the river Ferro.

The river networks were digitalized on 1:25 000 scale maps produced by the Italian Military Geographic Institute (Istituto Geografico Militare), through the aerial photo restitution technique. In the maps, the river networks are represented with blue lines. The blue lines were manually digitalized, obtaining a set of network points (net points) for each river network. The average manual digitalization step corresponded to about 5 m on the real scale; hereinafter, it will be referred to as a "random step," and the obtained net points will be called "randomly selected points."

The Corace river network (Fig. 1) was analyzed also at different constant digitalization steps (respectively 5, 8, and 15 m referred to the real scale), using AUTOCAD, in order to study the influence of the spatial resolution on the multifractal spectrum.

The Ferro braided channels (Fig. 2) were digitalized from 1:10 000 scale maps using AUTOCAD, with constant steps of respectively 2, 4, 5, and 8 m referred to the real scale. The average width of the river is about 370 m; at the downstream end, it is about 700 m.

Table I relates to the river networks. For each data set, it shows the total number of net points, N_t, the drainage area of the river basins, A, the number of net points per unit area, N_t/A, and some results which will be illustrated in the next paragraphs. Table II relates to the braided channels. For each data set, it shows the total number of net points, N_t, the length of the river reach, L, the number of net points per unit length, N_t/L, and some results which will be illustrated in the next paragraphs.

As stated in Sec. II, in the FMA the mass $p=N/N_t$ is the ratio between the constant number of points falling inside the generic cell and the total number of points in the set. However, numerically it is more convenient to work with nonnormalized quantities, since the use of integer numbers instead of real numbers increases the computational speed and the precision of results. Therefore, we carried out the calculations by using, instead of p, the constant number of points inside each cell, N. This operation does not change the results, since the normalization factor N_t is constant for each set, but increases the numerical stability.

FIG. 1. Corace river network.

Having chosen $\tau_q \in [-15, 10]$, for each value of τ_q we fixed the decreasing set of values of N with an exponential scale, ranging from the total number of net points, N_t, down to 1, the minimum possible value. Then, for each river network the scaling of $\ln M(\varepsilon_i, \tau_q)$ vs $\ln N$ was obtained. For example, Figs. 3(a)–3(c) show the scaling curves for τ_q

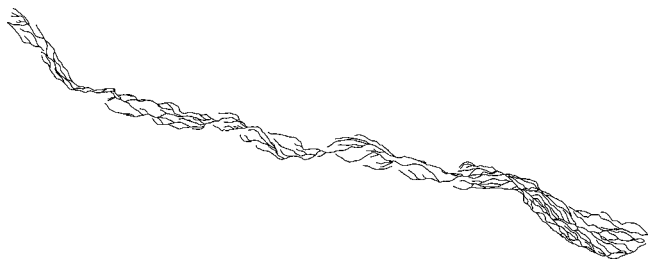

FIG. 2. Ferro braided channels.

TABLE I. Results of fixed-mass multifractal analysis (river networks).

River	Step (m)	N_t	A (km^2)	N_t/A (km^{-2})	α_0	$f(\alpha_0)$
Ancinale	Random	19380	174	111	1.828±0.006	1.807±0.006
Corace	Random	255885	294	870	1.834±0.001	1.805±0.011
	5	255137	294	868	1.844±0.001	1.820±0.009
	8	157183	294	535	1.850±0.002	1.827±0.008
	15	80894	294	275	1.859±0.003	1.839±0.007
Crati	Random	276121	2448	113	2.003±0.013	1.904±0.019
Petrace	Random	30039	407	74	1.873±0.004	1.833±0.011
Trionto	Random	61167	288	212	1.895±0.006	1.844±0.005
	Min	19380	174	74	1.828±0.006	1.805±0.011
	Average	140024	532	387	1.873±0.005	1.835±0.010
	Max	276121	2448	870	2.003±0.013	1.904±0.019

$=-15$ and 10 for all the random-step river networks and for the constant-step Corace river network and Ferro braided channels, respectively. For $\tau_q=-15$ to 10, we found the portions of the scaling curves where the least-square regression straight lines have the highest correlation coefficient, with slopes $(1-q)$, for all the data sets. In order to determine the error bars, we assessed the uncertainties of the slopes $(1-q)$ of the scaling curves and then performed the error propagation on the Lipschitz-Hölder exponents, α_q, and on the multifractal spectra, $f(\alpha_q)$. The sequences of the mass exponents, with the related error bars, are shown in Fig. 4, where only the Ancinale river network is presented as an example of random-step river networks (very similar results were obtained for the remaining random-step river networks). The multifractal spectra, computed from Eq. (4), are shown in Fig. 5 with the corresponding error bars.

Tables I and II show the Lipschitz-Hölder exponent α_0 and the fractal dimension $f(\alpha_0)$, with the corresponding errors, for the river networks and the braided channels, respectively. Also the minimum, average, and maximum values of the variables are shown.

IV. DISCUSSION

The interpolation of the τ_q values is usually performed with polynomials of second to seventh order in the case of river network analysis [15,23]. In the present analysis second- to third-order polynomials were selected, obtaining coefficients of determination equal to 1.00 and permitting the assessment of well-shaped multifractal spectra, without external points, which appeared if different order polynomials were used.

The positive moment orders, $q>0$, were assessed for $\tau_q=-1$ to 10; they ranged from 0.44 to 7.22 in the case of the river networks (random step), from 0.45 to 6.96 in the case of the Corace river network (different constant steps), and from 0.42 to 7.33 in the case of the Ferro braided channels (different constant steps). In particular, the above range limits were found to be almost constant at different steps (both random and constant).

The negative moment orders, $q<0$, were assessed in the whole range $\tau_q=-15$ to -2 for the random-step Ancinale river network ($q=-5.74$ to -0.11) and the constant-step Corace river network ($q=-6.68$ to -0.09) and Ferro braided channels ($q=-6.74$ to -0.15). In fact, in the case of the remaining random-step river networks the scaling curves showed some oscillations for $\tau_q<0$ [see Fig. 3(a)], preventing the assessment of the slope $(1-q)$ of the linear part of the curve. Therefore, the ranges of $\tau_q<0$ and $q<0$ were narrower in the case of the remaining random-step river networks ($\tau_q=-6$ to -2 and $q=-2.11$ to -0.05). Consequently, except for the Ancinale river network, the right part of the multifractal spectrum, $f(\alpha_q)$, was assessed better in the case of constant spatial resolutions (see Fig. 5). It is to be noted

TABLE II. Results of fixed-mass multifractal analysis (braided channels).

River reach	Step (m)	N_t	L (km)	N_t/L (km^{-1})	α_0	$f(\alpha_0)$
Ferro	2	32006	10	3201	1.763±0.001	1.729±0.005
	4	15892	10	1589	1.764±0.001	1.732±0.005
	5	12664	10	1266	1.769±0.001	1.738±0.003
	8	7838	10	784	1.770±0.001	1.741±0.004
	Min	7838		784	1.763±0.001	1.729±0.005
	Average	17100		1710	1.767±0.001	1.735±0.004
	Max	32006		3201	1.770±0.001	1.741±0.004

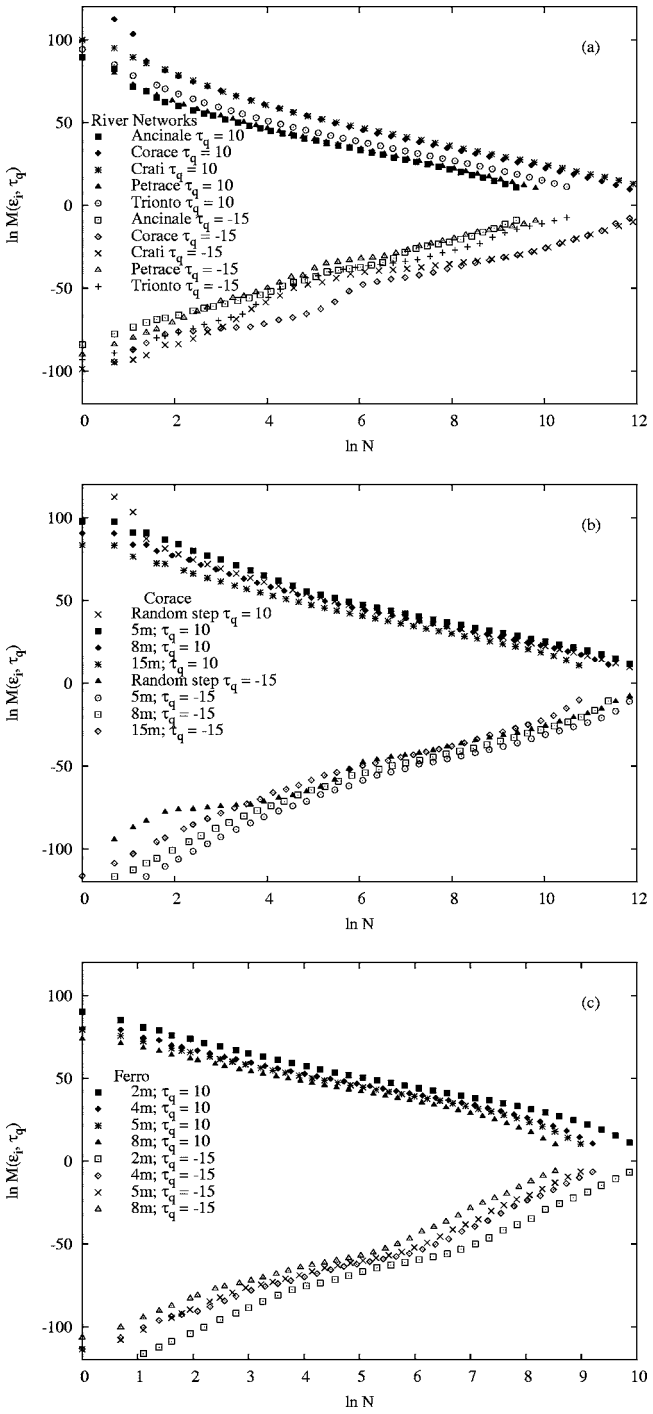

FIG. 3. Scaling curves (a) for the river networks with randomly selected points; (b) for the Corace river network at different spatial resolutions; (c) for the Ferro braided channels at different spatial resolutions.

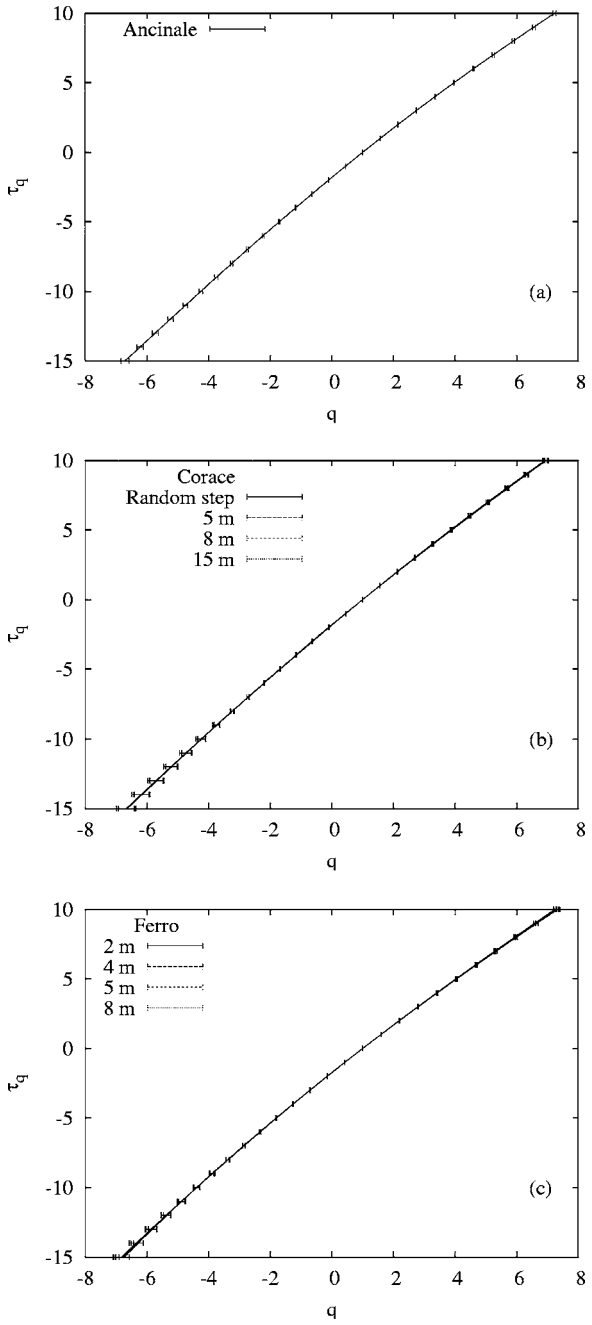

FIG. 4. Sequences of the mass exponents with error bars (a) for the Ancinale river network (resolution of about 5 m, randomly selected points); (b) for the Corace river network at different spatial resolutions; (c) for the Ferro braided channels at different spatial resolutions.

that the oscillations in the scaling curves were less than those found in the applications of the FSA [15].

For the river networks, the total number of net points ranged from 19 380 to 276 121, with average 140 024; the number of net points per unit area ranged from 74 to 870, with average 387 (see Table I). With respect to the braided channels, the total number of net points ranged from 7838 to 32 006, with average 17 100; the number of net points per unit length ranged from 784 to 3201, with average 1710 (see Table II). These numbers of net points permitted the assessment of the multifractal spectra in the ranges of moment orders reported above. The computational time (using a pentium IV processor) increased nonlinearly with N_t, ranging from 2 min to about 12 h.

For the random-step river networks, the range of variability of the spectrum peaks, $f(\alpha_0)$, was from 1.805 to 1.904, with average 1.835, while the Lipschitz-Hölder exponent α_0 ranged from 1.828 to 2.003, with average 1.873 (Table I).

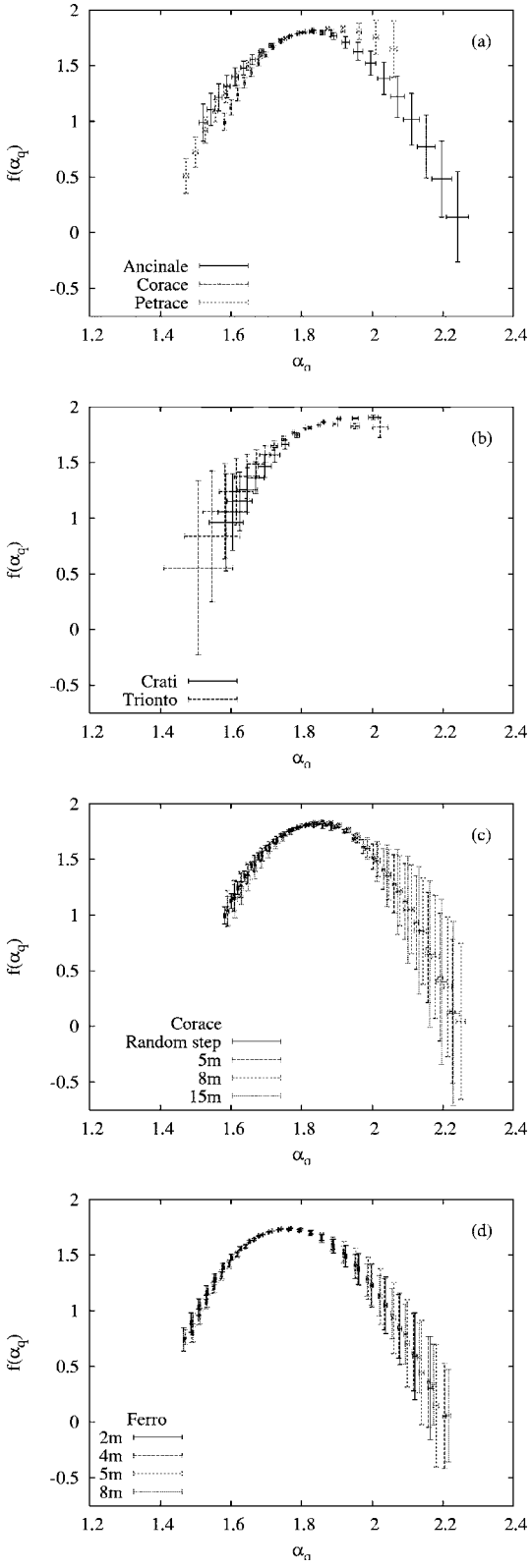

FIG. 5. Multifractal spectra with error bars (a) for the Ancinale, Corace, and Petrace river networks (resolution of about 5 m, randomly selected points); (b) for the Crati and Trionto river networks (resolution of about 5 m, randomly selected points); (c) for the Corace river network at different spatial resolutions; (d) for the Ferro braided channels at different spatial resolutions.

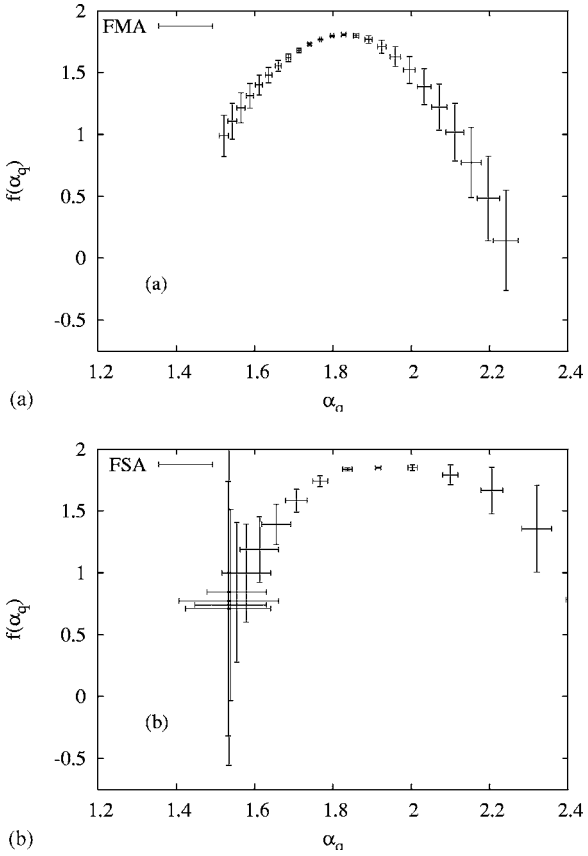

FIG. 6. Comparison between the multifractal spectra with error bars of the Ancinale river network (resolution of about 5 m, randomly selected points), obtained with (a) FMA and (b) FSA, respectively.

Similar results were obtained using FSAs [15], and the variability may be attributed to the different lithologic characteristics of the rocks on which the river networks are developed [23]. Nevertheless, the FMA applications produced shorter error bars than the FSA ones (see, e.g., Fig. 6). Regarding the applications to braided channels, we obtained values of $f(\alpha_0)$ from 1.729 to 1.741, with average 1.735, and of α_0 from 1.763 to 1.770, with average 1.767 (Table II). The errors on α_0 and $f(\alpha_0)$ were always modest; in particular, they were greater for river networks than for braided channels. The error bars increased for high absolute values of q (see Fig. 5). The spectra confirmed the hypotheses that the analyzed river networks and braided channels were multifractals and nonplane-filling structures $[f(\alpha_0)<2]$, as found in previous works for river networks only [15,23], in contrast with the findings of other authors in different contexts, where braided rivers of superconducting vortices were found to be multifractals with $D_{q=0}=2$ [24].

The influence of the spatial resolution on the multifractal spectrum was modest in the case of constant-step data sets (see Fig. 5). In fact, the $f(\alpha_0)$ values ranged from 1.820 to 1.839 for the Corace river network and from 1.729 to 1.741 for the Ferro braided channels, with relative differences of 1.0% and 0.7%, respectively. For the Lipschitz-Hölder exponents the relative differences ranged from 0.8% to 0.4%. For the Corace river network, the random step produced values

of $f(\alpha_0)$ and α_0 always out of the ranges obtained with constant steps, with minimum relative differences (with respect to the closest values obtained with constant steps) of 0.5% for α_0 and 0.8% for $f(\alpha_0)$, but without significant changes in the spectrum [see Fig. 5(c)].

V. CONCLUSIONS

A FMA was applied to river networks and braided channels. The analyzed data sets were shown to be multifractal and non-plane-filling structures, confirming previous results of FSA applications to river networks only. Therefore the results showed that braided channels, in spite of their different complexity with respect to river networks, exhibit an analogous multifractal behavior.

The implemented FMA was able to reconstruct the multifractal spectra for both positive and negative moment orders of probabilities, in particular in the case of constant digitalization step and with the correct choice of the polynomials interpolating the τ_q values. The spatial resolution of the data set was found not to exert a strong influence on the values of the Lipschitz-Hölder exponents and of the support dimensions, even if a constant digitalization step improved the results.

The FMA performance turned out to be better than the FSA ones in two respects: (1) the scaling curves oscillated less in the case of the FMA than in the case of the FSA for negative moment orders of probabilities; (2) the FMA multifractal spectra presented shorter error bars than the FSA ones. Therefore, the use of FMA improved the assessment of the generalized fractal dimensions, which is a point of great concern in the simulation of flood events with multifractal hydrologic models.

[1] B. B. Mandelbrot, in *Statistical Models and Turbulence*, edited by M. Rosenblatt and C. Van Atta, Lecture Notes in Physics Vol. 12 (Springer, Berlin, 1972), p. 333; J. Fluid Mech. **62**, 331 (1974); *The Fractal Geometry of Nature* (Freeman, New York, 1982).

[2] P. Grassberger, Phys. Lett. **97A**, 227 (1983).

[3] P. Grassberger and I. Procaccia, Phys. Rev. Lett. **50**, 346 (1983).

[4] H. G. E. Hentschel and I. Procaccia, Physica D **8**, 435 (1983).

[5] D. Schertzer and S. Lovejoy, in Proceedings of the Fourth Symposium on Turbulent Shear Flows, Karlsruhe, 1983 (unpublished), p. 11.1.

[6] X. J. Hou, R. Gilmore, G. Mindlin, and H. Solari, Phys. Lett. A **151**, 43 (1990).

[7] R. Badii and A. Politi, Phys. Rev. Lett. **52**, 1661 (1984); J. Stat. Phys. **40**, 725 (1985); for the measurement of the multifractal spectrum $f(\alpha_q)$ with the fixed-mass approach, see R. Badii and G. Broggi, Phys. Lett. A **131**, 339 (1988).

[8] U. Frisch and G. Parisi, in *Turbulence and Predictability in Geophysical Fluid Dynamics and Climate Dynamics*, edited by M. Ghil,Proceedings of the International School of Physics "Enrico Fermi," Course LXXXVIII, Amsterdam (North-Holland, New York, 1985), p. 84.

[9] E. Ijjasz-Vasquez, I. Rodriguez-Iturbe, and R. L. Bras, Geomorphology **5**, 297 (1992); A. Rinaldo, I. Rodriguez-Iturbe, R. Rigon, R. L. Bras, E. Ijjasz-Vasquez, and A. Marani, Water Resour. Res. **28**, 2183 (1992); A. Rinaldo, I. Rodriguez-Iturbe, R. Rigon, E. Ijjasz-Vasquez, and R. L. Bras, Phys. Rev. Lett. **70**, 822 (1993); R. Rigon, A. Rinaldo, I. Rodriguez-Iturbe, R. L. Bras, and E. Ijjasz-Vasquez, Water Resour. Res. **29**, 1635 (1993); I. Rodriguez-Iturbe and A. Rinaldo, *Fractal River Basins: Chance and Self-Organization* (Cambridge University Press, New York, 1997).

[10] S. G. De Bartolo, M. Maiolo, M. Veltri, and P. Veltri, Idrotecnica **6**, 329 (1995) (in Italian); S. G. De Bartolo, S. Gabriele, and R. Gaudio, Hydrology Earth Syst. Sci. **4**, 105 (2000); S. G. De Bartolo, M. Veltri, and L. Primavera, L'Acqua **6**, 9 (2003) (in Italian); S. G. De Bartolo, R. Gaudio, and S. Gabriele, Water Resour. Res. **40**, W02201 (2004); S. G. De Bartolo, M. Veltri, and L. Primavera, J. Hydrol. **322**, 181 (2006).

[11] S. G. De Bartolo, L. Ambrosio, L. Primavera, and M. Veltri in *Atti del Convegno La Difesa Idraulica del Territorio, Trieste*, 2003 edited by E. Caroni, V. Fiorotto, A. Mancinelli, and P. Salandin (Tergeste, Trieste), p. 47 (in Italian). The multifractal instantaneous unit hydrograph permits a good assessment of observed hydrographs. It is based on a Γ-type function, expressing the relation of the IUH as a function of time, through a time scale parameter and the maximum Lipschitz-Hölder exponent, by virtue of the link of the last parameter with the minimum probability and the resolution at which the measure is performed.

[12] M. Veltri, S. Gabriele, S. G. De Bartolo, R. Gaudio, and L. Primavera, in *Workshop Modelli Matematici per la Simulazione di Catastrofi Idrogeologiche, Rende, 2004*, edited by P. Versace (AGM Castrovillari,Castrovillary CS, Italy, 2005), p. 79.

[13] P. Claps and G. Oliveto, Water Resour. Res. **32**, 3123 (1996).

[14] M. Veltri, P. Veltri, and M. Maiolo, J. Hydrol. **187**, 137 (1996).

[15] For negative moment orders of probability (right side of the spectrum), see S. G. De Bartolo, M. Veltri, and L. Primavera, L'Acqua **6**, 9 (2003) (in Italian); S. G. De Bartolo, R. Gaudio, and S. Gabriele, Water Resour. Res. **40**, W02201 (2004); S. G. De Bartolo, M. Veltri, and L. Primavera, J. Hydrol. **322**, 181 (2006).

[16] J. Mach, F. Mas, and F. Sagués, J. Phys. A **28**, 5607 (1995).

[17] T. Tel, Á Fülöp, and T. Vicsek, Physica A **159**, 155 (1989); T. Vicsek, *ibid.* **168**, 490 (1990); T. Vicsek, F. Family, and P. Meakin, Europhys. Lett. **12**, 217 (1990).

[18] K. Pawelzik and H. G. Schuster, Phys. Rev. A **35**, 481 (1987).

[19] For the application of the sandbox method to river networks, see S. G. De Bartolo, R. Gaudio, and S. Gabriele, Water Resour. Res. **40**, W02201 (2004); for the application of the generalized correlation integral method to river networks, see S. G. De Bartolo, M. Veltri, and L. Primavera, J. Hydrol. **322**, 181 (2006); for the aspects concerning the border effects, see S. G. De Bartolo, S. Gabriele, and R. Gaudio, Hydrology Earth

Syst. Sci. **4**, 105 (2000).
[20] R. Albert and A.-L. Barabási, Rev. Mod. Phys. **74**, 47 (2002).
[21] For the FSA formalism, see K. J. Falconer, *Fractal Geometry: Mathematical Foundations and Applications* (John Wiley & Sons, Chichester, 1990); also *Techniques in Fractal Geometry* (John Wiley & Sons, Chichester, 1997); for the FMA formalism, see J. Mach, F. Mas, and F. Sagués, J. Phys. A **28**, 5607 (1995); R. Pastor-Satorras, Phys. Rev. E **56**, 5284 (1997).
[22] T. C. Halsey, M. H. Jensen, L. P. Kadanoff, I. Procaccia, and B. I. Shraiman, Phys. Rev. A **33**, 1141 (1986).
[23] R. Gaudio, S. G. De Bartolo, L. Primavera, S. Gabriele, and M. Veltri, J. Hydrol. DOI: 10.1016/j. jhydrol.2005.11.025 (to be published).
[24] K. E. Bassler, M. Paczuski, and G. F. Reiter, Phys. Rev. Lett. **83**, 3956 (1999).